

Physical conditions in potential sources of ultra-high-energy cosmic rays. I. Updated Hillas plot and radiation-loss constraints

Ksenia Ptitsyna¹ and Sergey Troitsky²

¹ M.V. Lomonosov Moscow State University, Moscow 119992, Russia

² Institute for Nuclear Research of the Russian Academy of Sciences,
60th October Anniversary Prospect 7a, 117312, Moscow, Russia

E-mail: `st@ms2.inr.ac.ru`

Abstract. We review basic constraints on the acceleration of ultra-high-energy cosmic rays (UHECRs) in astrophysical sources, namely the geometrical (Hillas) criterion and restrictions from radiation losses in different acceleration regimes. Using the latest available astrophysical data, we redraw the Hillas plot and figure out potential UHECR accelerators. For the acceleration in central engines of active galactic nuclei, we constrain the maximal UHECR energy for a given black-hole mass. Among active galaxies, only the most powerful ones, radio galaxies and blazars, are able to accelerate protons to UHE, though acceleration of heavier nuclei is possible in much more abundant lower-power Seyfert galaxies.

PACS number: 98.70.Sa

Contents

1	Introduction	2
2	General constraints from geometry and radiation	4
2.1	The Hillas criterion	4
2.2	Radiation losses	5
2.3	Different acceleration regimes	5
2.3.1	Diffusive acceleration.	6
2.3.2	One-shot acceleration with synchrotron-dominated losses.	6
2.3.3	One-shot acceleration with curvature-dominated losses.	6
2.4	Summary of results for the maximal energy	7
3	Magnetic fields in particular sources	7
3.1	Neutron stars, pulsars and magnetars	7
3.2	Supermassive black holes and their environment	8
3.3	Jets and outflows of active galaxies	11
3.4	Jet knots, hot spots and lobes of powerful active galaxies	12
3.5	Star formation regions and starburst galaxies	13
3.6	Gamma-ray bursts	13
3.7	Galaxy clusters, superclusters and voids	15
4	Summary and discussion	16
5	Conclusions	20

1. Introduction

The origin of ultra-high-energy (UHE; energy $\mathcal{E} \gtrsim 10^{19}$ eV) cosmic rays (CRs) remains unknown despite decades of intense studies (see e.g. Ref. [1] for a comprehensive review and Ref. [2] for a recent pedagogical introduction). Recent studies, notably the observation of the Greisen–Zatsepin–Kusmin [3, 4] cutoff by the HiRes experiment [5], further supported by results of the Pierre Auger observatory (PAO) [6], suggest that at least a large fraction of UHECRs is accelerated in cosmologically distant astrophysical sources. The birth of (scientific) UHECR astronomy, however, awaits our firm understanding of energies and primary composition of the observed cosmic rays as well as identification of at least one astrophysical object where these particles are accelerated.

From the experimental side, UHECR physics suffers from the lack of understanding of hadronic interactions at energies beyond the reach of terrestrial accelerators, and hence of the air-shower development [7]. For instance, the Pierre Auger Collaboration performed two different analyses of their data [6, 8] and obtained a disagreement of 30 per cent in the energy scale [8]; none of the two results agrees with the shower-development

models [8]. While recent results [9] of PAO and of the Yakutsk experiment [10] suggest the presence of a significant fraction of heavy nuclei among the UHECR primaries, HiRes results both on composition [11] and on the spectrum [5], as well as the Auger interpretation of their anisotropy results [12] favour proton dominance.

The interest to UHECR astronomy has been revived by these latter Auger claims [12, 13] of a strong anisotropy in the arrival directions of the most energetic CRs. Soon after publication, the conclusions of Ref. [12] have been subjected both to different tests with the same data [14] and to similar tests with the HiRes data [15]; these tests disfavoured the interpretation of Refs. [12, 13] (while, despite the difference in the energy scale and in the angular resolution, the Yakutsk data confirm [16] the Auger results). Other interpretations have been suggested and discussed [14, 17, 18, 19, 20, 21, 22, 23, 24, 25, 26, 27].

Given the experimental ambiguities, it is important to understand theoretically, which astrophysical objects may serve as UHECR accelerators. It has been understood long ago that the UHECR sources should be distinguished objects with extreme physical conditions. One simple criterion is the geometrical one: the particle should not leave the accelerator before it gains the required energy. Presumably, the particle is accelerated by the electric field and confined by the magnetic one; then the geometrical criterion is expressed in terms of the particle's Larmor radius which should not exceed the linear size of the accelerator (see, e.g., Ref. [28]). In the context of UHECRs, this condition is recognized as the Hillas criterion [29] and is often presented graphically in terms of the Hillas plot where the accelerator size R and the magnetic field B are plotted. We note that even quite recent reviews use either cut-and-pasted or slightly refurbished versions of the original 25-years-old plot. However, astrophysics experienced enormous progress, if not a revolution, during these decades. One of the aims of this study is to give an updated version of the Hillas plot with references to either – when possible – measurements or estimates of the magnetic fields and sizes of potential astrophysical accelerators. The most important update corresponds to a wide variety of active galaxies whose sizes and magnetic fields differ by many orders of magnitude from one object to another so that some of them may, while most of them may not, accelerate particles to UHE.

Another restriction on the cosmic-ray accelerators is posed by the radiation losses which inevitably accompany the acceleration of a charged particle. The corresponding constraints were studied, in particular, in Refs. [29, 30, 31, 32]. The radiation losses depend on the particular field configuration and the maximal achievable energy of a particle in the loss-limited regime depends on the acceleration mechanism. Restricting to particular mechanisms or particular field configurations may result in would-be contradictory results, cf. Refs. [31, 32]. In this work, we review the radiation-loss constraint for different cases; they further limit the acceptable region on the updated Hillas plot. These general constraints are applied to active galaxies correlated with the Auger events in an accompanying paper [33].

The rest of the paper is organised as follows. In Sec. 2, we review constraints on

potential UHE accelerators, that is model-independent Hillas geometrical constraint and limitations due to radiation losses for particular acceleration mechanisms. In Sec. 3, we take advantage of the modern astrophysical data and redraw the Hillas plot supplemented by the radiation-loss constraints. Our results are summarized and discussed in Sec. 4 while brief conclusions are given in Sec. 5.

2. General constraints from geometry and radiation

An accelerator of UHECR particles should satisfy several general constraints which may be briefly summarized as follows:

- **geometry** — the accelerated particle should be kept inside the source while being accelerated;
- **power** — the source should possess the required amount of energy to give it to accelerated particles;
- **radiation losses** — the energy lost by a particle for radiation in the accelerating field should not exceed the energy gain;
- **interaction losses** — the energy lost by a particle in interactions with other particles should not exceed the energy gain;
- **emissivity** — the total number (density) and power of sources should be able to provide the observed UHECR flux;
- **accompanying radiation** of photons, neutrinos and low-energy cosmic rays should not exceed the observed fluxes, both for a given source and for the diffuse background (in particular, the ensemble of sources should reproduce the observed cosmic-ray *spectrum*[‡]).

The primary concern of this paper is the geometrical and radiation-loss constraints (others are briefly quoted when relevant); both restrict the magnetic field and the size of the accelerator and can be graphically represented on the Hillas plot.

2.1. The Hillas criterion

The Larmor radius of a particle does not exceed the accelerator size, otherwise the particle escapes the accelerator and cannot gain energy further. This Hillas criterion sets the limit

$$\mathcal{E} \leq \mathcal{E}_H = qBR \quad (1)$$

for the energy \mathcal{E} gained by a particle with charge q in the region of size R with the magnetic field B .

[‡] We note that the spectrum of cosmic rays accelerated in a particular source may be very different from the spectrum observed at the Earth, cf. Ref. [34].

2.2. Radiation losses

While Eq. (1) is a necessary limit, more stringent ones may arise from the energy losses: the maximal energy $\mathcal{E}_{\text{loss}}$ a particle can get in an accelerator of infinite size is determined by the condition

$$\frac{d\mathcal{E}^{(+)}}{dt} = -\frac{d\mathcal{E}^{(-)}}{dt}, \quad (2)$$

where the energy gain rate in the effective electric field $E = \eta B$ is (in the particle-physics $c = 1$ units)

$$\frac{d\mathcal{E}^{(+)}}{dt} = q\eta B \quad (3)$$

and we hereafter use the efficiency coefficient $\eta = 1$ to obtain conservative limits for a given magnetic field (the electric fields in astrophysical objects are much less studied observationally compared to the magnetic ones, but it is always expected that $E \ll B$). Depending on particular conditions in the accelerator, the maximal energy \mathcal{E}_{max} of a particle is limited either by geometrical or by energy-loss arguments:

$$\mathcal{E}_{\text{max}} = \min \{ \mathcal{E}_{\text{H}}, \mathcal{E}_{\text{loss}} \}.$$

The general expression for the radiation losses for a particle with velocity \mathbf{v} moving in arbitrary electric \mathbf{E} and magnetic \mathbf{B} fields reads (see e.g. Ref. [35])

$$-\frac{d\mathcal{E}^{(-)}}{dt} = \frac{2}{3} \frac{q^4}{m^2} \mathcal{E}^2 \left((\mathbf{E} + [\mathbf{v} \times \mathbf{B}])^2 - (\mathbf{E}\mathbf{v})^2 \right),$$

where q and m are the particle's charge and mass, respectively. By making use of the relativistic equations of motion, it can be conveniently rewritten [36] as

$$-\frac{d\mathcal{E}^{(-)}}{dt} = \frac{2}{3} q^2 \frac{1}{(1 - v^2)^3} (w_{\parallel}^2 + w_{\perp}^2 (1 - v^2)),$$

where the acceleration \mathbf{w} of a particle is separated into parallel w_{\parallel} and perpendicular w_{\perp} components with respect to \mathbf{v} . It is apparent that the second term (the so-called curvature radiation) is suppressed with respect to the first one (synchrotron radiation) by an extra power of $(1 - v^2)$ and therefore may be neglected in the ultrarelativistic regime unless the synchrotron term is zero or very small itself. The synchrotron losses are dominant for any generic field configuration; however, in a very specific regime $\mathbf{v} \parallel \mathbf{E} \parallel \mathbf{B}$ they vanish, and the losses are then determined by the curvature radiation.

2.3. Different acceleration regimes

Known acceleration scenarios may be divided into diffusive and inductive, or “one-shot”, mechanisms (see e.g. Ref. [29]). In the most common diffusive acceleration scenario, a particle is moving inside the accelerator and gets a hit from time to time, increasing its energy either in a collision with a shock wave or by crossing a boundary between layers with different velocities, or even by transforming itself into another particle (see e.g. Ref. [37] and references therein). In inductive mechanisms, the particle is

accelerated by the large-scale electric field continuously and then leaves the accelerator. For our purposes, it is convenient to separate the inductive-acceleration scenarios into two groups, depending on whether the configuration of the accelerating field corresponds to synchrotron- or curvature-dominated losses.

2.3.1. Diffusive acceleration. Since the particle is accelerated episodically but radiates continuously, the losses in this regime are the most serious. This scenario cannot be realized in strongly ordered field configurations with curvature-dominated losses, therefore the losses are determined by the synchrotron case,

$$-\frac{d\mathcal{E}^{(-)}}{dt} = \frac{2}{3} \frac{q^4}{m^4} \mathcal{E}^2 B^2 \quad (\text{synchrotron}). \quad (4)$$

This regime has been studied in Ref. [32] where it has been shown that no matter how strongly the particle is accelerated with a hit, the maximal energy is limited by

$$\mathcal{E}_d \simeq \frac{3}{2} \frac{m^4}{q^4} B^{-2} R^{-1}.$$

Diffusive mechanisms are quite generic and may work in every realistic environment which can host, e.g., a shock wave.

2.3.2. One-shot acceleration with synchrotron-dominated losses. In this regime, the energy loss rate is given by Eq. (4) and Eq. (2) gives the maximal energy

$$E_s = \sqrt{\frac{3}{2}} \frac{m^2}{q^{3/2}} B^{-1/2}.$$

This acceleration mechanism requires ordered fields throughout the acceleration site; its practical realization for UHECR may work in jets of powerful active galaxies.

2.3.3. One-shot acceleration with curvature-dominated losses. The energy loss rate is determined by

$$-\frac{d\mathcal{E}^{(-)}}{dt} = \frac{2}{3} \frac{q^2}{r^2} \left(\frac{\mathcal{E}}{m} \right)^4 \quad (\text{curvature}), \quad (5)$$

where r is the curvature radius of the field lines which is supposed to be of order of the accelerator size and Eq. (2) results in the maximal energy

$$\mathcal{E}_c = \left(\frac{3}{2} \right)^{1/4} \frac{m}{q^{1/4}} B^{1/4} R^{1/2}.$$

This mechanism requires ordered fields of very specific configurations which, however, may be present in the immediate vicinity of neutron stars and black holes (see e.g. Refs. [38, 39, 40, 41] for discussion of the corresponding acceleration mechanisms).

2.4. Summary of results for the maximal energy

Let us summarize the expressions for the maximal energy \mathcal{E}_{\max} (in the comoving frame) attainable by a nuclei with atomic number Z and mass A in the accelerator of size R filled with magnetic field B , for different acceleration regimes:

$$\mathcal{E}_{\max}(B, R) = \begin{cases} \mathcal{E}_{\text{H}}(B, R), & B \leq B_0(R); \\ \mathcal{E}_{\text{loss}}(B, R), & B > B_0(R), \end{cases}$$

where

$$B_0(R) = 3.16 \times 10^{-3} \text{ G} \frac{A^{4/3}}{Z^{5/3}} \left(\frac{R}{\text{kpc}} \right)^{-2/3},$$

the Hillas constraint is

$$\mathcal{E}_{\text{H}}(B, R) = 9.25 \times 10^{23} \text{ eV} \ Z \left(\frac{R}{\text{kpc}} \right) \left(\frac{B}{\text{G}} \right),$$

and the radiation-loss constraints are

$$\mathcal{E}_{\text{loss}}(B, R) = \mathcal{E}_{\text{d}}(B, R) = 2.91 \times 10^{16} \text{ eV} \frac{A^4}{Z^4} \left(\frac{R}{\text{kpc}} \right)^{-1} \left(\frac{B}{\text{G}} \right)^{-2}$$

for diffusive acceleration,

$$\mathcal{E}_{\text{loss}}(B, R) = \mathcal{E}_{\text{s}}(B, R) = 1.64 \times 10^{20} \text{ eV} \frac{A^2}{Z^{3/2}} \left(\frac{B}{\text{G}} \right)^{-1/2}$$

for inductive acceleration with synchrotron-dominated losses and

$$\mathcal{E}_{\text{loss}}(B, R) = \mathcal{E}_{\text{c}}(B, R) = 1.23 \times 10^{22} \text{ eV} \frac{A}{Z^{1/4}} \left(\frac{R}{\text{kpc}} \right)^{1/2} \left(\frac{B}{\text{G}} \right)^{1/4}$$

for inductive acceleration with curvature-dominated losses. Applications to particular objects and graphical representations of the constraints will follow in Sec. 4 (see in particular Figs. 8 – 12).

3. Magnetic fields in particular sources

A number of astrophysical sources have been proposed where acceleration of cosmic rays up to the highest energies can take place (see e.g. Refs. [42, 43] for reviews and summary). In this section, we review experimental information on their magnetic fields in order to put them in proper places on the Hillas plot. General methods of astrophysical magnetic-field studies are discussed e.g. in Refs. [44, 45]; however, a much wider variety of them is used for studies of individual sources.

3.1. Neutron stars, pulsars and magnetars

Neutron stars host the highest known magnetic fields in the Universe. In particular, anomalous X-ray pulsars and magnetars may possess kilometer-scale fields $B \sim 10^{15} \text{ G}$ and higher while normal neutron stars have $B \sim (10^{11} \div 10^{12}) \text{ G}$. Observational evidence for these high fields is discussed e.g. in Sec. 6.3 of Ref. [46]. We note also a direct

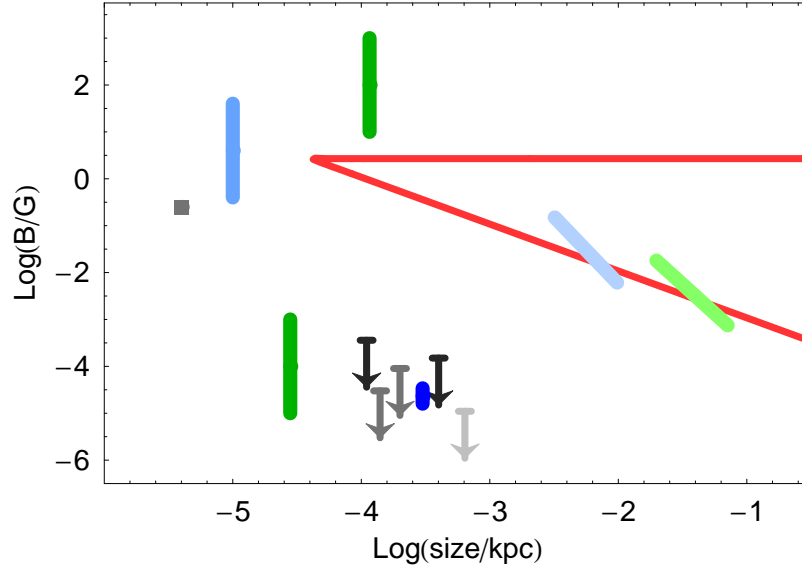


Figure 1. The size-field diagram for central regions of active galactic nuclei. Grey colors correspond to Seyfert galaxies, blue colors correspond to FRI radio galaxies, green colors correspond to FRII radio galaxies and quasars. Arrows: upper limits from the Zeeman splitting in megamasers (light grey, Ref. [49]; medium grey, Ref. [50]; dark grey, Ref. [51]). Dark blue vertical error bar: Faraday rotation measurements, Ref. [52]. The grey box [53], light blue vertical [54], dark green [55] and diagonal [56] error bars correspond to the measurements by the synchrotron self-absorption method (see text). The allowed region for acceleration of 10^{20} eV protons is located between thick red lines (the lower line corresponds to the Hillas limit, the upper one corresponds to the radiation-loss limit for one-shot acceleration with synchrotron-dominated losses).

observational method to measure B in neutron stars, observation of spectral lines giving evidence for resonant Compton scattering at cyclotron frequency in the high-field media, see e.g. Ref. [47] for normal neutron stars and Ref. [48] for anomalous X-ray pulsars.

3.2. Supermassive black holes and their environment

Measurements of magnetic fields in the central regions of galaxies have been performed by means of the following methods (see Fig. 1 for particular results and references).

1. Synchrotron self-absorption. Under certain conditions, the low-energy cutoff in the spectrum of a compact source may be detected and its shape may be proven to correspond to the absorption of synchrotron photons on themselves. If this is the case, then the magnetic-field strength may be determined by means of the Slysh formula [57] or its modifications. The method works best of all for strong radio sources with resolved nuclear components.

2. Polarimetry. Measurements of the Faraday rotation and of resulting depolarization give estimates of the magnetic field provided the plasma density is known from independent observations.

3. Zeeman effect in megamasers. Megamasers are compact sources of coherent radiation in molecular clouds inside or around the accretion disk. Current precision allows to put very stringent constraints on the magnetic fields in these regions from non-observation of the Zeeman splitting in megamasers in nearby Seyfert galaxies.

4. The iron K_α line. Measurements of the width and shape of this X-ray line may provide important information about circumnuclear dynamics; in particular, it may be used to estimate the magnetic field, though present constraints are quite weak [58].

All these direct measurements, however, cannot probe the most interesting region in the immediate vicinity of the central black hole, a few Schwarzschild radii (R_S) from the center. This region is particularly important because theoretically motivated configurations of electric and magnetic fields may allow for negligible synchrotron radiation of accelerated particles and thus for (relatively weak) curvature-radiation losses. Lack of our understanding of the field structure in the accretion disk is transformed into uncertainties in the inferred magnetic fields B_{BH} at the black-hole horizon (see e.g. Ref. [59] for a summary of models used for this extrapolation). Direct estimates of B_{BH} are therefore not only scarce but also model-dependent.

On the other hand, parameters of the environment of a black hole and in particular the value of B_{BH} depend strongly on the black-hole mass M_{BH} . A conservative upper limit on B_{BH} follows from the condition that the maximal rate of extraction of the rotational energy of a black hole does not exceed the Eddington luminosity [60],

$$B_{\text{BH}} \lesssim 10^4 \left(\frac{M_{\text{BH}}}{10^9 M_\odot} \right)^{-1/2} \text{ G}. \quad (6)$$

Quite old but popular models estimate the $M_{\text{BH}} - B_{\text{BH}}$ relation from the pressure balance (radiation pressure equals to the magnetic-viscosity pressure) [61, 62]:

$$B_{\text{BH}} \sim 10^8 \left(\frac{M_{\text{BH}}}{M_\odot} \right)^{-1/2} \text{ G}. \quad (7)$$

An efficient method to constrain the relation between M_{BH} and B_{BH} was found in Ref. [63] in the frameworks of a particular theoretical model. It gives somewhat lower values of B_{BH} than Eq. (7); the best fit is

$$\log \left(\frac{B_{\text{BH}}}{\text{G}} \right) = (9.26 \pm 0.39) - (0.81 \pm 0.05) \log \left(\frac{M_{\text{BH}}}{M_\odot} \right), \quad (8)$$

where the central values of the coefficients are taken from Ref. [63] and the error bars are estimated by us from their data. For two cases when rather firm and model-independent values of B_{BH} could be inferred from the observations (synchrotron self absorption measured at different radii down to 0.1 pc and extrapolated to R_S , Ref. [56]), we estimated the corresponding M_{BH} and found that both values are in a good agreement with Eq. (8), though precision is quite low.

Estimates of B_{BH} versus M_{BH} are summarized in Fig. 2. We will use the upper limit, Eq. (6), to estimate B_{BH} for a given M_{BH} ; we note however that realistic values of B_{BH} are 1...2 orders of magnitude lower. Since for the curvature-dominated radiation

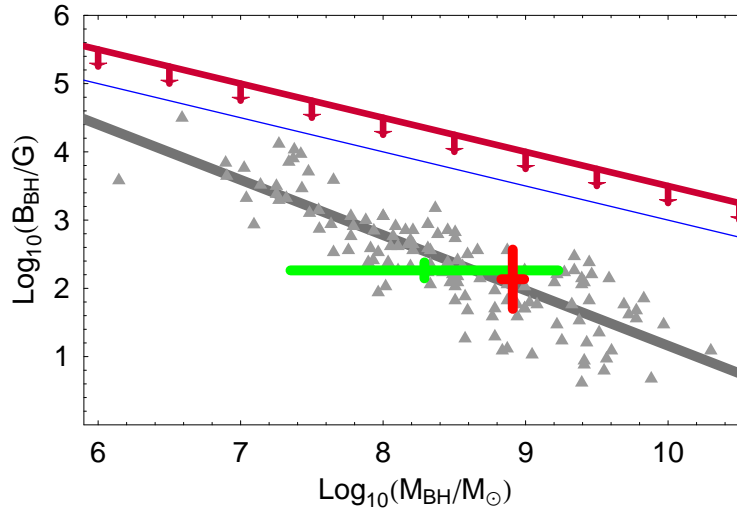


Figure 2. Magnetic field B_{BH} at the black-hole horizon versus the black hole mass M_{BH} . Triangles are model-dependent estimates of Ref. [63] and the grey line represents their best fit, Eq. (8). Two points with error bars correspond to experimental estimates of B_{BH} , Ref. [56], using the synchrotron self-absorption method (M_{BH} estimated by us using the stellar velocity dispersion from HyperLEDA [64] (red, FRI radio galaxy 3C 465) and 2MASS K_s magnitude quoted in NED [65] (green, FRII radio galaxy 3C 111); see Ref. [33] for details). Thin blue line corresponds to the Shakura–Sunyaev estimate, Eq. (7). Thick red line represents the Znajek upper limit, Eq. (6). This conservative upper limit is used in our estimates of the maximal cosmic-ray energy.

losses higher B always results in higher \mathcal{E}_{max} , this assumption is conservative for our purposes.

The size R of the potential acceleration region (that is, the region occupied by $\mathbf{E} \parallel \mathbf{B}$ fields suitable for curvature-dominated losses) is of order R_S ; therefore both R and B are governed by a single parameter M_{BH} , so one may express the maximal energy through M_{BH} using results of Sec. 2.4. Assuming

$$R \sim 5R_S \approx 5 \times 10^{-5} \text{ pc } \frac{M_{\text{BH}}}{10^8 M_\odot},$$

one finds that for any reasonable M_{BH} (ranging from $\sim 10^6 M_\odot$ for normal galaxies through $(10^7 \dots 10^8) M_\odot$ for Seyfert galaxies to $(10^9 \dots 10^{10}) M_\odot$ for powerful radio galaxies and quasars) the maximal energy is determined by radiation losses rather than by the Hillas condition and equals to

$$\mathcal{E}_{\text{max}} = \mathcal{E}_c \simeq 3.7 \times 10^{19} \text{ eV } \frac{A}{Z^{1/4}} \left(\frac{M_{\text{BH}}}{10^8 M_\odot} \right)^{3/8}. \quad (9)$$

This general constraint is presented in Fig. 3 for different nuclei (A, Z); for comparison, results of numerical simulations of particle acceleration near a supermassive black hole [41] are also plotted.

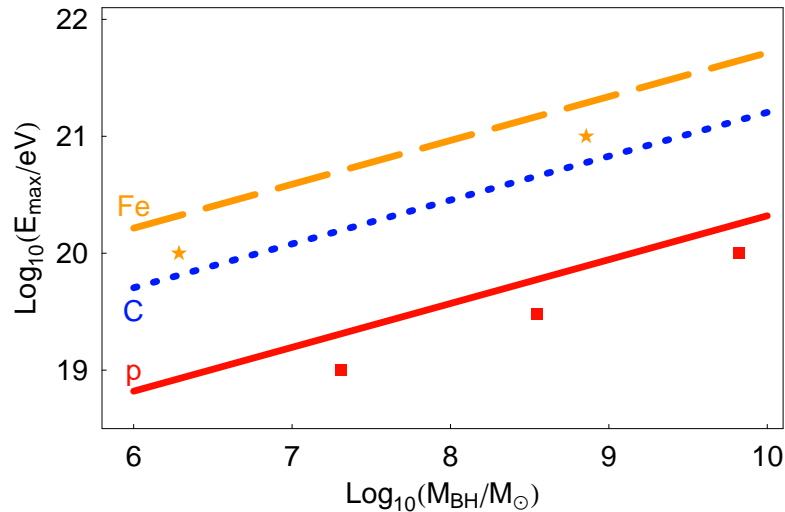


Figure 3. Maximal attainable energy of protons (red solid line), carbon nuclei (blue dotted line) and iron nuclei (orange dashed line) for acceleration with curvature-dominated losses near a supermassive black hole, Eq. (9). The maximal energy obtained in numerical simulations in a particular mechanism [41] is shown by red boxes (protons) and orange stars (iron nuclei); these data were obtained from Figs. 5 and 10 of Ref. [41] and Eq. (6) of this paper.

3.3. Jets and outflows of active galaxies

Active galactic nuclei fuel large-scale (from sub-parsec to kiloparsec and even Megaparsec length) extended more or less linear jets. Revolutionary progress in the angular resolution of radio (sub-milliarcsecond) and X-ray (sub-arcsecond) imaging allowed for detailed studies of them; physical conditions in jets are often modelled with a high level of confidence.

Seyfert galaxies possess extended structures which are often non-collimated (opening angle of 45° or more) and are found to be non-relativistic; they are sometimes determined as “outflows”, reserving the term “jets” to strongly collimated relativistic flows. X-ray emission from these outflows, when present, is well described by thermal radiation (sometimes associated with star-forming regions).

Relativistic jets reveal themselves in non-thermal X-ray emission studied now in great detail (see e.g. Ref. [66] for a review). The jets are spatially resolved into components; in nearby jets (Cen A) inner and outer layers and bright knots are resolved. To the best of current understanding, all jets are fuelled by the central black hole; the energy flux is dominated by the magnetic-field energy at sub-parsec scales but becomes particle-dominated at parsec scales. Low-luminosity sources (FR I radio galaxies and BL Lacs) are perfectly described by the synchrotron models; their jets are decelerated by entrainment of gas and dissipate in the end. High-power FR II and quasar jets bring their energy flux directly to their terminal hot spots and require additional (e.g. Compton) component to describe their spectra. Comparison of radio to X-ray observations gives

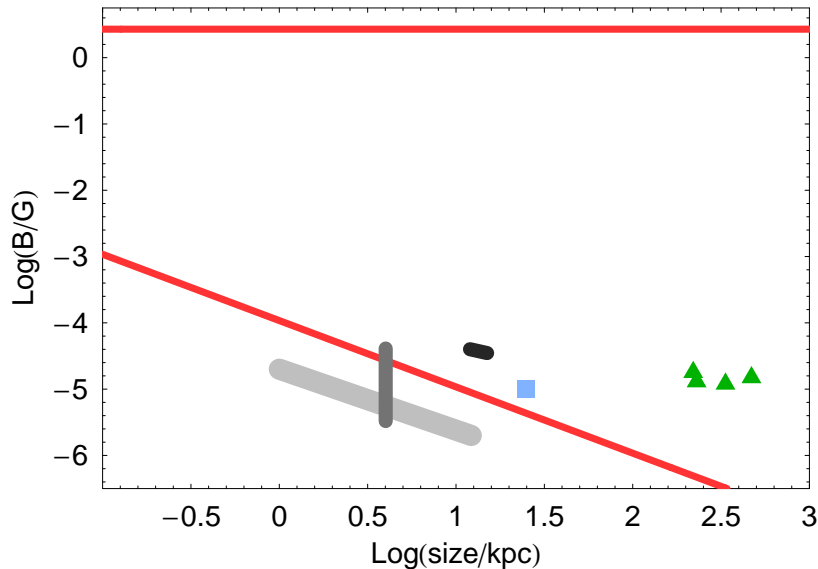


Figure 4. The size-field diagram for jets and outflows of individual active galaxies. Grey colors correspond to Seyfert galaxies, data from Refs. [67] (light-grey diagonal line), [68] (grey vertical error bar), [69] (dark grey diagonal). Blue box corresponds to FR I radio galaxy [70]; green triangles represent quasar jets [71]. The allowed region for acceleration of 10^{20} eV protons is located between thick red lines (the lower line corresponds to the Hillas limit, the upper one corresponds to the radiation-loss limit for inductive acceleration with synchrotron-dominated losses).

rather firm evidence to the origin of the emission of FR I jets from accelerated particles and to acceleration of these particles not only in a finite number of shocks but also by means of some distributed mechanism along the jet. Quite rarely, relativistic jets are present in exceptionally powerful Seyfert galaxies; in these cases, they have properties very similar to FR I jets. Models of multifrequency spectra allow to constrain the magnetic field, the key parameter of the synchrotron radiation. Some of these estimates are presented in Fig. 4. In some cases, existence of ordered fields through the jet was proven, so inductive acceleration may be possible.

3.4. Jet knots, hot spots and lobes of powerful active galaxies

When a relativistic jet is present, it may be accompanied by internal shock regions (knots), terminal shock regions (hot spots) and extended regions in the intergalactic space fuelled by the jet after its termination (lobes). These regions are absent in low-power active galaxies (knots are observed mostly in jets of FR I radio galaxies and quasars, lobes are typical for radio galaxies, hot spots are present in the most powerful FR II radio galaxies only). Magnetic fields may be determined either by X-ray synchrotron observations alone (assuming equipartition) or by combined multifrequency observations of both synchrotron and Compton radiations (allowing to relax the equipartition assumption which occurs, in the end, a good approximation, see e.g.

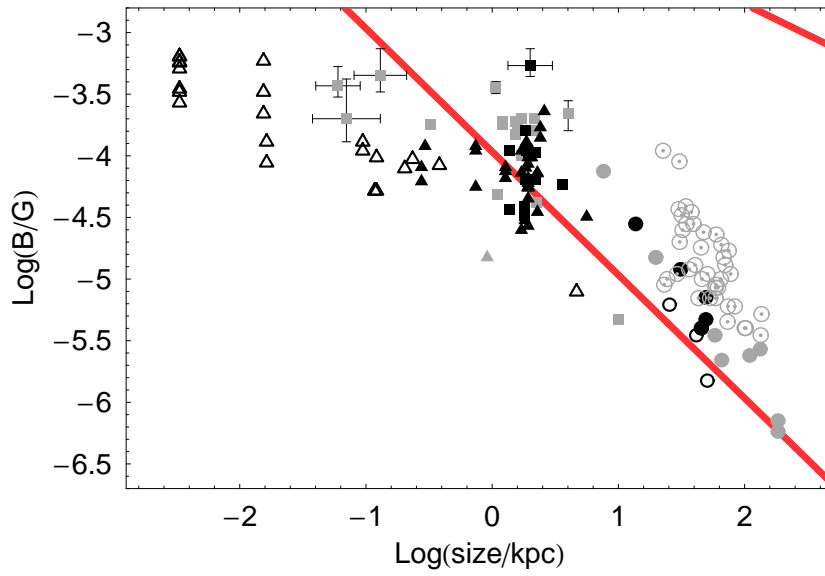


Figure 5. The size-field diagram for knots (triangles), hot spots (boxes) and lobes (circles) of individual powerful active galaxies. Filled black symbols correspond to quasars and blazars, filled grey symbols correspond to FR II radio galaxies, empty symbols correspond to FR I radio galaxies (data from Ref. [73], X-ray observations assuming equipartition); boxes with error bars represent the “best-guess” estimates of Ref. [74]; dotted grey circles correspond to FR II lobes studied in Ref. [75] (comparison of radio and X-ray observations without the equipartition assumption). The allowed region for acceleration of 10^{20} eV protons is located between thick red lines (the lower line corresponds to the Hillas limit, the upper one corresponds to the radiation-loss limit for diffusive acceleration).

Ref. [72]). A summary of measurements is given in Fig. 5.

3.5. Star formation regions and starburst galaxies

Measurements of the magnetic field in Galactic star-forming regions becomes possible with the Zeeman splitting in masers in circumstellar disks. Though these regions in our Galaxy have never been considered as possible sites of UHECR acceleration, these measurements may give some hints to the fields in larger star-forming regions in starburst galaxies, where particles could be accelerated to very high energies e.g. in shocks from subsequent supernova explosions; magnetic fields in these extragalactic sites are measured indirectly. A summary of measurements is given in Fig. 6; a number of arguments in favour of higher (equipartition) fields in starburst galaxies were presented in Ref. [81] while continuity with the Galactic measurements may support lower (minimal-energy) estimates.

3.6. Gamma-ray bursts

Estimates of the magnetic field in gamma-ray bursts (GRBs) assume that the origin of both the prompt gamma-ray and afterglow emissions is the synchrotron radiation of

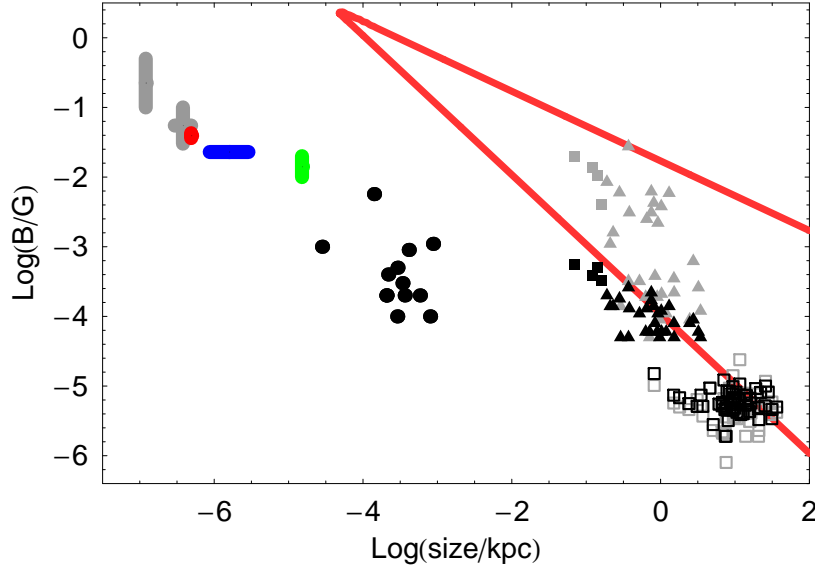


Figure 6. The size-field diagram for Galactic star-forming regions ($R \lesssim \text{pc}$) and starburst galaxies ($R \gtrsim 0.1 \text{ kpc}$). Thick (error-bar) lines correspond to measurements of the Zeeman splitting in masers (grey, Ref. [76]; red, Ref. [77]; blue, Ref. [78]; green, Ref. [79]). Black dots represent results of submillimeter imaging polarimetry of Ref. [80]. Data for normal (empty boxes), starburst (triangles) and extreme starburst (filled boxes) galaxies are taken from Ref. [81]; black symbols correspond to the minimal-energy field estimates while grey symbols correspond to equipartition field estimates. The allowed region for acceleration of 10^{20} eV protons is located between thick red lines (the lower line corresponds to the Hillas limit, the upper one corresponds to the radiation-loss limit for diffusive acceleration).

relativistic electrons. This assumption is supported by measurements of the afterglow spectra and lightcurves and by observation of the strongly polarized prompt emission (see Ref. [82] for discussion and references). Ref. [82] quotes $B \sim 10^6 \text{ G}$ for $R \sim (10^{13} \div 10^{15}) \text{ cm}$ (prompt emission) and $B \sim 1 \text{ G}$ for $R \sim (10^{16} \div 10^{18}) \text{ cm}$ (afterglow). Another, somewhat higher field estimate may be obtained following Ref. [31] from the total luminosity of a GRB, assuming that the magnetic-field energy \mathcal{E}_m is a fraction $\epsilon_m < 1$ of the radiation energy \mathcal{E}_{rad} . To obtain order-of-magnitude estimates of the magnetic field, we assume a spherical source of the radius $R/2$ filled with magnetic field B , so that the energy of the magnetic field is $\mathcal{E}_m \sim \pi R^3 B^2/6$. The energy of the radiation field may be estimated as $\mathcal{E}_{\text{rad}} \sim R d\mathcal{E}_{\text{rad}}/dt$, where the energy loss $d\mathcal{E}_{\text{rad}}/dt = L$, the bolometric luminosity of the source. We obtain

$$B \sim \sqrt{\frac{6L\epsilon_m}{\pi}} \frac{1}{R} \approx 250 \text{ G} \left(\frac{L}{10^{52} \text{ erg/s}} \right)^{1/2} \left(\frac{R}{\text{pc}} \right)^{-1} \epsilon_m. \quad (10)$$

Suggested mechanisms of UHECR acceleration in GRB operate either at $R \sim (10^{-9} \div 10^{-6}) \text{ pc}$ (internal shocks [83]) or at $R \sim (10^{-3} \div 10^{-2}) \text{ pc}$ (external shock [84]) while the luminosities of the most GRBs are $L \sim (10^{51} \div 10^{53}) \text{ erg/s}$ [85].

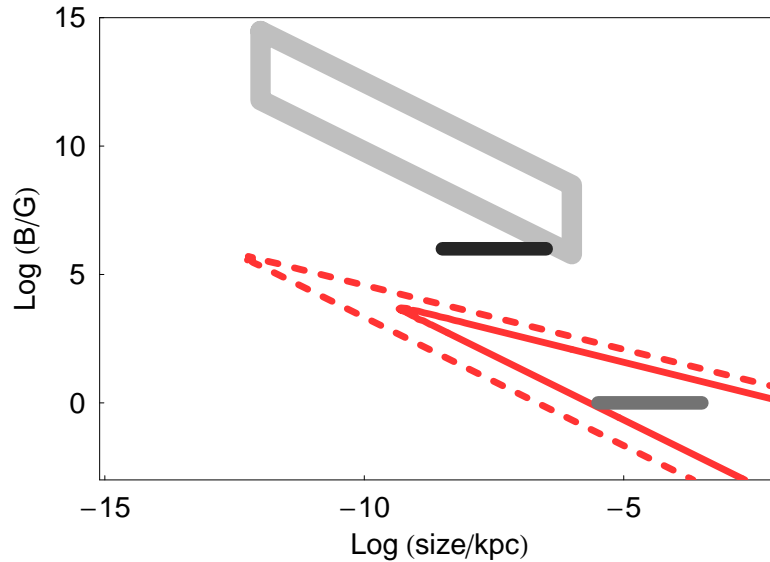


Figure 7. The size-field diagram for gamma-ray bursts. The area bound by the grey line represents estimates of Eq. (10) for typical values of parameters. Horizontal lines represent estimates of Ref. [82] which assume the synchrotron origin for the prompt emission (dark grey) and the afterglow (light grey). The allowed region for acceleration of 10^{20} eV protons is located between dashed red lines for $\Gamma = 500$ and between full red lines for $\Gamma = 50$ (the lower lines correspond to the Hillas limit, the upper ones correspond to the radiation-loss limit for diffusive acceleration).

Within the scope of this paper, we may estimate the maximal energy \mathcal{E}_{\max} of accelerated particles in the comoving frame following equations of Sec. 4 for shock (diffusive) acceleration. The GRB shells are however ultrarelativistic ($\Gamma \sim 100$, see e.g. Ref. [86]) and we have to multiply the comoving-frame \mathcal{E}_{\max} by Γ to get the maximal rest-frame energy. Results are presented in Fig. 7 which, for the GRB case, is more instructive than the summary plots of Sec. 4. We note that at large Γ , the maximal energy may be limited by interactions with thermal photon field (not taken into account in the present work) and *decreases* as Γ^{-1} at large Γ [31].

3.7. Galaxy clusters, superclusters and voids

Information about cluster magnetic fields comes mostly from observations of their extended radio, and sometimes X-ray, emission. These observations are reviewed e.g. in Refs. [87, 88]. Estimates based on equipartition, as well as those assuming Compton scattering on CMB photons, favour values of $B \sim (0.1 \div 1) \mu\text{G}$ at megaparsec scales; Faraday rotation measurements favour somewhat higher fields, $B \sim (1 \div 5) \mu\text{G}$. Model-dependent numerical simulations remain the main source of information about magnetic fields at the supercluster scales ($R \sim 100$ Mpc), especially in voids. Estimates vary between $B \sim 10^{-11}$ G [89] and $B \sim 10^{-8}$ G [90].

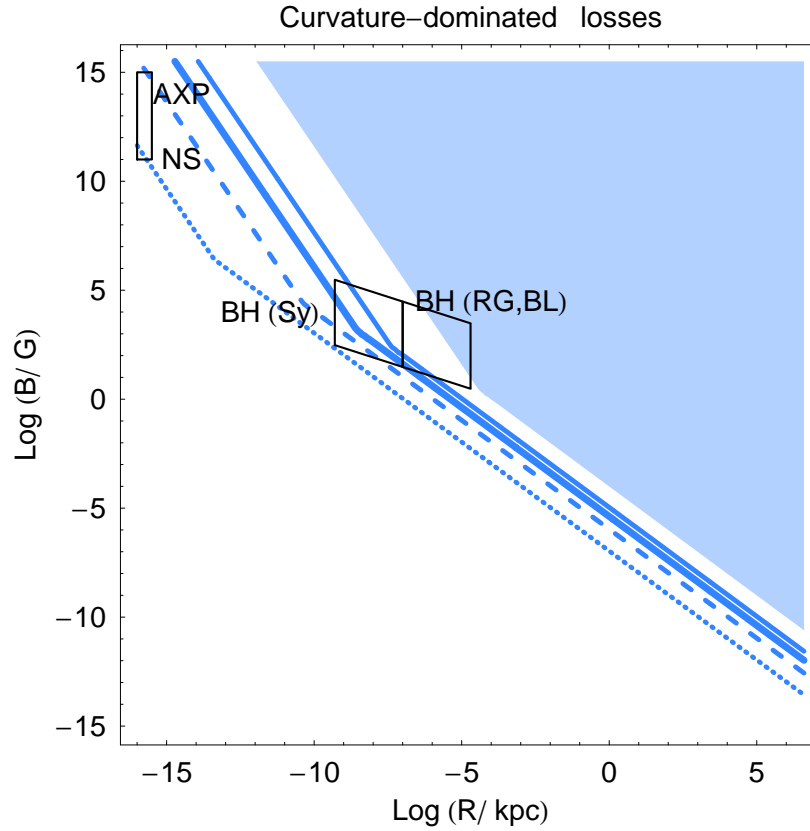


Figure 8. The size-field plot with constraints from geometry and radiation losses for the regime where losses are dominated by curvature radiation. These are minimal possible losses and these constraints are therefore the most weak. Boxes denote parameter regions for objects in which conditions for this loss regime may be satisfied, that is immediate neighbourhood of neutron stars (NS), anomalous X-ray pulsars and magnetars (AXP) and of supermassive central black holes (BH) of active galactic nuclei, from low-power Seyfert galaxies (Sy) to powerful radio galaxies (RG) and blazars (BL). The shaded area corresponds to the parameter region where acceleration of protons to 10^{20} eV is possible. Lines bind from below the allowed regions for 10^{19} eV protons (thin full line), 10^{20} eV iron nuclei (thick full line), 10^{18} eV protons (dashed line) and 10^{17} eV protons (dotted line). Right-hand parts of the lines represent the Hillas constraint while left-hand (steeper) parts represent the radiation-loss constraint.

4. Summary and discussion

Based on the data collected in Sec. 3 and on the limits on the maximal energy, Sec. 2.4, we redraw here the Hillas plot supplemented with radiation-loss constraints. Figures 8 – 10 give constraints for particular acceleration regimes while Figs. 11, 12 represent our updated summary Hillas plots.

The weakest possible constraints (for inductive acceleration with curvature-dominated losses) are presented in Fig. 8. Constraints for inductive acceleration with synchrotron-dominated losses, applicable mostly to inner and outer jets of active galaxies, are given in Fig. 9, while constraints for the most general diffusive acceleration

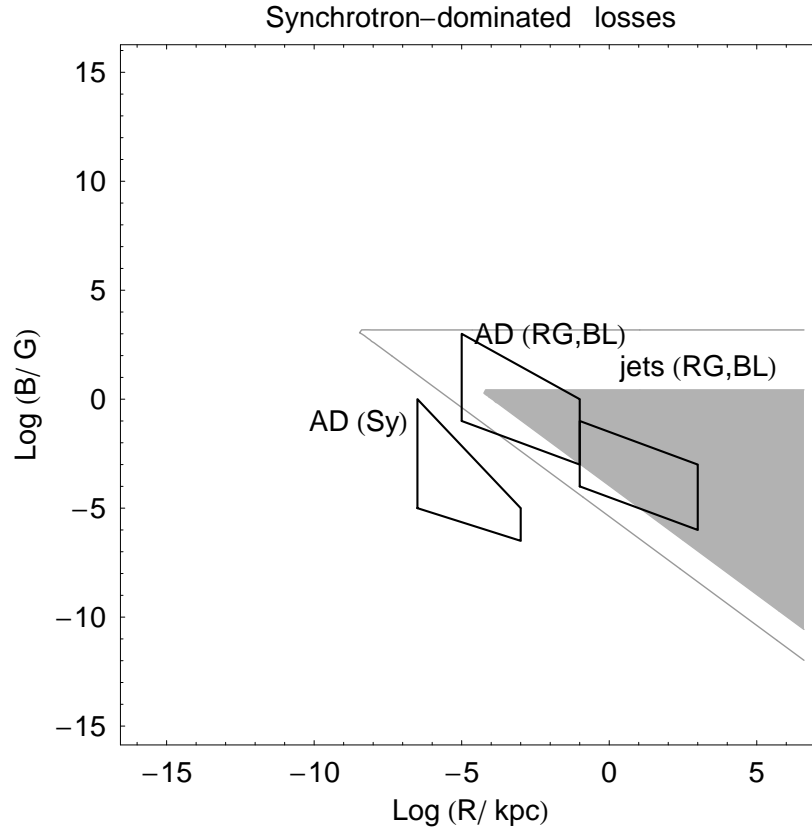


Figure 9. The size-field plot with constraints from geometry and radiation losses for the regime of one-shot acceleration with synchrotron-dominated losses. Boxes denote parameter regions for objects in which conditions for this loss regime may be satisfied, that is central parsecs (AD) of active galaxies (low-power Seyfert galaxies (Sy) and powerful radio galaxies (RG) and blazars (BL)) and relativistic jets of powerful active galaxies. The shaded area corresponds to the parameter region where acceleration of protons to 10^{20} eV is possible. The line binds the allowed regions for 10^{20} eV iron nuclei. Lower lines represent the Hillas constraint while upper (horizontal) lines represent the radiation-loss constraint. All quantities are given in the comoving frame, so the maximal energy for jets should be multiplied by the bulk Lorentz factor of the jet, typically ~ 10 for leptonic jets and ~ 100 for hadronic jets [31].

are presented in Fig. 10. Figure 11 represents our version of the Hillas plot with constraints for 10^{20} eV protons. Figure 12 is the same plot but for 10^{20} eV iron nuclei.

The constraints discussed here and expressed in terms of the Hillas plot are necessary, but they should be supplemented by other limits (listed in the beginning of Sec. 2). We note that in estimation of the maximal attainable energy, important constraints are put by interactions of accelerated particles with ambient photons. In particular, interaction with the cosmic microwave background is important for large, $R \gtrsim \text{Mpc}$, sources (lobes of radio galaxies, clusters and voids), while interaction with the internal source radiation field is important for ultraluminous sources (GRB and

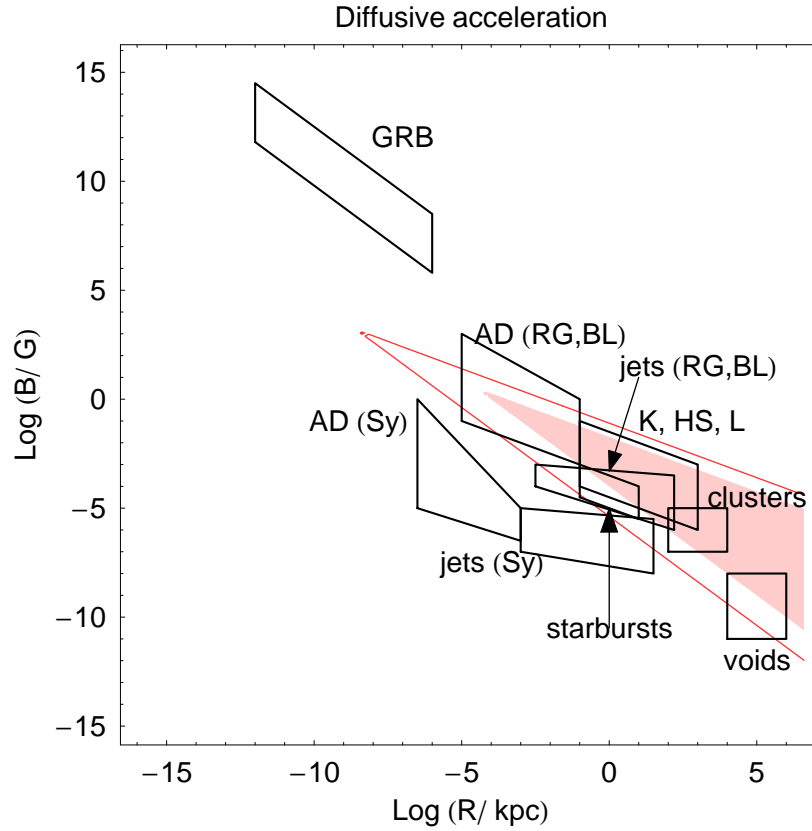


Figure 10. The size-field plot with constraints from geometry and radiation losses for the regime of diffusive acceleration with synchrotron-dominated losses. Boxes denote parameter regions for objects in which conditions for this loss regime may be satisfied, that is central parsecs (AD) of active galaxies (low-power Seyfert galaxies (Sy) and powerful radio galaxies (RG) and blazars (BL)), relativistic jets, knots (K), hot spots (HS) and lobes (L) of powerful active galaxies (RG and BL); non-relativistic jets of low-power galaxies (Sy); starburst galaxies; gamma-ray bursts (GRB); galaxy clusters and intercluster voids. The shaded area corresponds to the parameter region where acceleration of protons to 10^{20} eV is possible. The line binds the allowed regions for 10^{20} eV iron nuclei. Lower lines represent the Hillas constraint while upper lines represent the radiation-loss constraint. All quantities are given in the comoving frame, so the maximal energy for jets and shells of GRBs should be multiplied by the bulk Lorentz factor, typically ~ 10 for leptonic jets and ~ 100 for hadronic jets and GRBs [31].

AGN). These constraints, considered elsewhere, further restrict the number of potential UHECR accelerators.

The maximal energy for the supermassive black holes is readily expressed in terms of a single parameter, the black-hole mass M_{BH} . We used the upper limit on the magnetic field, B_{BH} , which is most likely one or two orders of magnitude higher than the actual values, so that our estimate, Eq. (9), is robust. It depends weakly ($\sqrt{R/R_S}$) on the assumed size of the acceleration region.

While we tried to make all constraints as robust as possible, it is clear that they

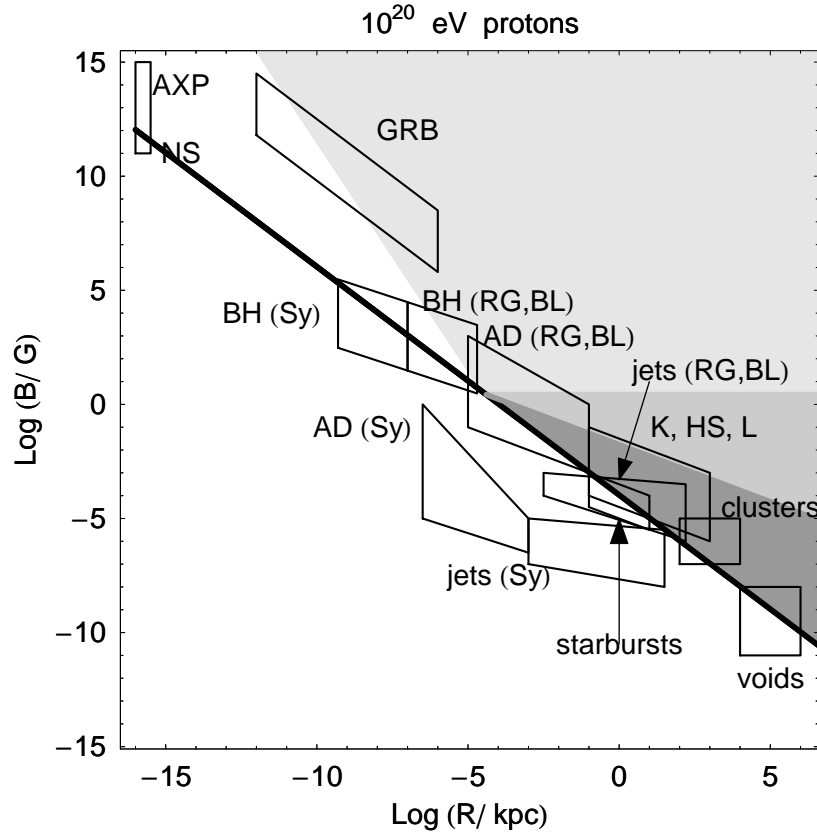


Figure 11. The Hillas plot with constraints from geometry and radiation losses for 10^{20} eV protons. The thick line represents the lower boundary of the area allowed by the Hillas criterion. Shaded areas are allowed by the radiation-loss constraints as well: light grey corresponds to one-shot acceleration in curvature-dominated regime only; grey allows also for one-shot acceleration in synchrotron-dominated regime; dark grey allows for both one-shot and diffusive (e.g. shock) acceleration. See captions to Figs. 8, 9, 10 for notation of boxes corresponding to potential sources.

should be considered as order-of-magnitude estimates (in fact, typical precision of the magnetic-field determination is an order of magnitude) and, for individual unusual field configurations, can be quantitatively violated. An example of such a configuration is a linear accelerator with curvature radius R_c of field lines exceeding the size of the source R ; then R should be substituted by R_c in Eq. (5).

One of our most important conclusions is that low-power active galaxies (e.g. Seyfert galaxies) cannot accelerate protons to energies $\gtrsim 5 \times 10^{19}$ eV. They can, in principle, accelerate protons to $\sim 10^{18}$ eV and heavy nuclei to $\sim 10^{20}$ eV near central supermassive black holes, if interactions with ambient photons are weak enough. Though heavy nuclei are much less abundant than protons, Seyfert galaxies themselves are much more abundant, and hence typically close to the observer, than powerful radio galaxies and blazars, so that their population can contribute to UHECR spectrum.

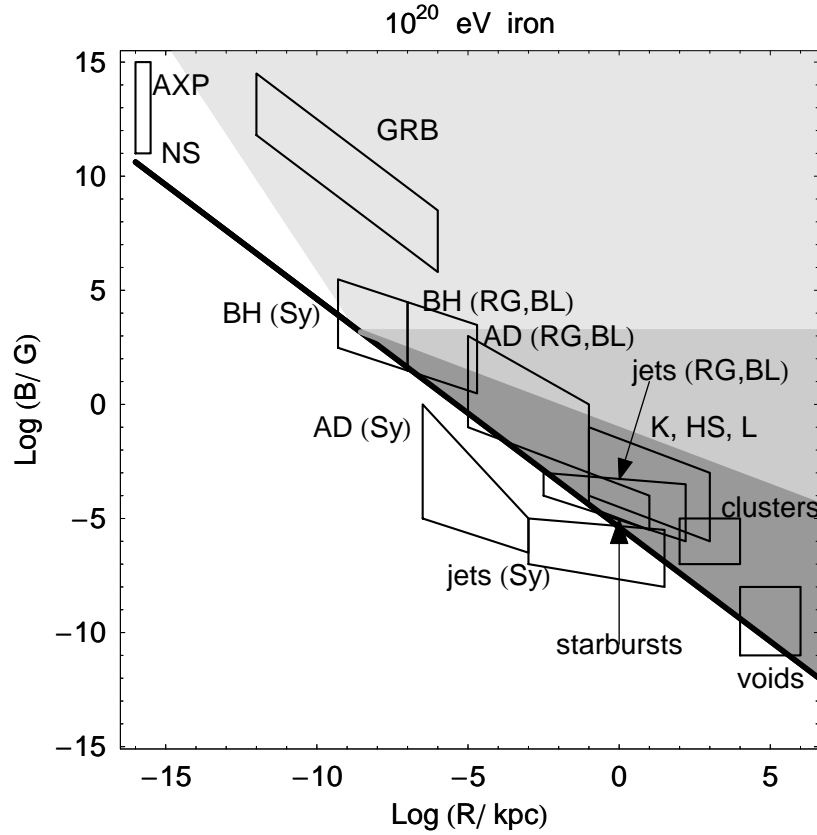


Figure 12. The same as Fig. 11 but for 10^{20} eV iron nuclei. The most important difference with Fig. 11 is that acceleration of iron nuclei to 10^{20} eV is possible (unlike for protons) in low-power active galaxies (e.g. Seyfert galaxies).

5. Conclusions

We reviewed constraints on astrophysical UHE accelerators and presented the Hillas plot supplemented with radiation-loss constraints and updated with recent astrophysical data. Contrary to previous studies, we emphasised that active galaxies span a large area on the plot, and only the most powerful ones (radio galaxies, quasars and BL Lac type objects) are capable of acceleration of protons to UHE. If UHECR particles are accelerated close to the supermassive black holes in AGN, then most likely the mechanism is “one-shot” with energy losses dominated by the curvature radiation. Other potential UHE acceleration sites are jets, lobes, knots and hot spots of *powerful* active galaxies, starburst galaxies and shocks in galaxy clusters. Acceleration of particles in supercluster-scale shocks, gamma-ray bursts and inner part of AGN is subject to additional constraints from $p\gamma$ interactions not discussed here.

Unlike protons, heavy nuclei can be accelerated to UHE in circumnuclear regions of low-power active galaxies. Since these galaxies are abundant, this contribution to UHECR flux may be important, leading to a mixed primary cosmic-ray composition at highest energies.

Acknowledgments

The authors are indebted to D. Gorbunov, S. Gureev, V. Lukash, A. Neronov, S. Popov and D. Semikoz for helpful discussions. We acknowledge the use of online tools [64, 65]. The work of ST was supported in part by the grants RFBR 07-02-00820 and NS-7293.2006.2 (government contract 02.445.11.7370).

References

- [1] Nagano M and Watson A A, *Observations And Implications Of The Ultrahigh-Energy Cosmic Rays*, 2000, *Rev. Mod. Phys.* **72** 689
- [2] Kachelriess M, *Lecture notes on high energy cosmic rays*, 2008, arXiv:0801.4376 [astro-ph]
- [3] Greisen K, *End To The Cosmic Ray Spectrum?*, 1966 *Phys. Rev. Lett.* **16** 748
- [4] Zatsepin G T and Kuzmin V A, *Upper limit of the spectrum of cosmic rays*, 1966 *JETP Lett.* **4** 78 [*Pisma Zh. Eksp. Teor. Fiz.* **4** 114]
- [5] Abbasi R *et al.*, (The High Resolution Fly’s Eye Collaboration), *Observation of the GZK cutoff by the HiRes experiment*, 2008, *Phys. Rev. Lett.* **100** 101101 [arXiv:astro-ph/0703099]
- [6] The Pierre Auger Collaboration, *Observation of the suppression of the flux of cosmic rays above 4×10^{19} eV*, 2008, arXiv:0806.4302 [astro-ph]
- [7] Ostapchenko S S, *Simulations Of Cosmic Ray Interactions: Past, Present, And Future*, 2006 *J. Phys. Conf. Ser.* **47** 222
- [8] Engel R *et al.* (The Pierre Auger Collaboration), *Test of hadronic interaction models with data from the Pierre Auger Observatory*, 2007, arXiv:0706.1921 [astro-ph]
- [9] Unger M *et al.* (The Pierre Auger Collaboration), *Study of the Cosmic Ray Composition above 0.4 EeV using the Longitudinal Profiles of Showers observed at the Pierre Auger Observatory*, 2007, arXiv:0706.1495
- [10] Glushkov A V *et al.*, *Muon content of ultra-high-energy air showers: Yakutsk data versus simulations*, 2008, *JETP Lett.* **87** 190 [arXiv:0710.5508 [astro-ph]]
- [11] Abbasi R U *et al.* (The High Resolution Fly’s Eye Collaboration), *A study of the composition of ultra high energy cosmic rays using the High Resolution Fly’s Eye*, 2005, *Astrophys. J.* **622** 910 [arXiv:astro-ph/0407622]
- [12] Abraham J *et al.* (The Pierre Auger Collaboration), *Correlation of the highest energy cosmic rays with nearby extragalactic objects*, 2007, *Science* **318** 938 [arXiv:0711.2256].
- [13] Abraham J *et al.* (The Pierre Auger Collaboration), *Correlation of the highest-energy cosmic rays with the positions of nearby active galactic nuclei*, 2008, *Astropart. Phys.* **29** 188 [arXiv:0712.2843]
- [14] Gorbunov D *et al.*, *Comment on ‘Correlation of the Highest-Energy Cosmic Rays with Nearby Extragalactic Objects’*, 2008, *JETP Lett.* **87** 461 [arXiv:0711.4060]
- [15] Abbasi R U *et al.* (The High Resolution Fly’s Eye Collaboration), *Search for Correlations between HiRes Stereo Events and Active Galactic Nuclei*, 2008, arXiv:0804.0382 [astro-ph]
- [16] Ivanov A A, *A search for Extragalactic Sources of Ultrahigh-Energy Cosmic Rays*, 2008, *JETP Lett.* **87** 185 [arXiv:0803.0612 [astro-ph]]
- [17] Wibig T and Wolfendale A W, *Heavy Cosmic Ray Nuclei from Extragalactic Sources above ‘The Ankle’*, 2007, arXiv:0712.3403 [astro-ph]
- [18] Fargion D, *Light Nuclei solving Auger puzzles?*, 2008, arXiv:0801.0227 [astro-ph]
- [19] Kotera K and Lemoine M, *The optical depth of the Universe for ultra-high energy cosmic ray scattering in the magnetized large scale structure*, 2008, *Phys. Rev. D* **77** 123003 [arXiv:0801.1450 [astro-ph]]
- [20] Gorbunov D S *et al.*, *On the interpretation of the cosmic-ray anisotropy at ultra-high energies*, 2008, arXiv:0804.1088 [astro-ph]

- [21] Dermer C D, *The obscured gamma-ray and UHECR universe*, arXiv:0804.2466 [astro-ph]
- [22] Dedenko L G *et al.*, *The cosmic ray luminosity of the nearby active galactic nuclei*, 2008, arXiv:0804.4582 [astro-ph]
- [23] Moskalenko I V *et al.*, *On the Possible Association of Ultra High Energy Cosmic Rays with Nearby Active Galaxies*, 2008, arXiv:0805.1260 [astro-ph]
- [24] Stanev T, *A comment on the Auger events correlation with AGN*, 2008, arXiv:0805.1746 [astro-ph]
- [25] George M R *et al.*, *On Active Galactic Nuclei as Sources of Ultra-High Energy Cosmic Rays*, 2008, arXiv:0805.2053 [astro-ph]
- [26] Ghisellini G *et al.*, *Ultra-High Energy Cosmic Rays, Spiral galaxies and Magnetars*, 2008, arXiv:0806.2393 [astro-ph]
- [27] Nagar N M and Matulich J, *Ultra-High Energy Cosmic Rays Detected by the Pierre Auger Observatory: First Direct Evidence, and its Implications, that a Subset Originate in Nearby Radiogalaxies*, 2007, arXiv:0806.3220 [astro-ph]
- [28] Schlüter A und Biermann L, *Interstellare Magnetfelder*, 1950, *Z. Naturforsch.* **5a** 237
- [29] Hillas A M, *The origin of ultra-high-energy cosmic rays*, 1984, *Ann. Rev. Astron. Astrophys.* **22** 425
- [30] Protheroe R J, *Effect of energy losses and interactions during diffusive shock acceleration: Applications to SNR, AGN and UHE cosmic rays*, 2004, *Astropart. Phys.* **21** 415 [arXiv:astro-ph/0401523]
- [31] Aharonian F A, *Constraints on the extremely high-energy cosmic ray accelerators from classical electrodynamics*, 2002, *Phys. Rev.* **D66** 023005 [arXiv:astro-ph/0202229]
- [32] Medvedev M V, *A constraint on electromagnetic acceleration of highest energy cosmic rays*, 2003, *Phys. Rev.* **E67** 045401 [arXiv:astro-ph/0303271]
- [33] Gureev S and Troitsky S, *Physical conditions in potential sources of ultra-high-energy cosmic rays. II. Nearby active galaxies correlated with Auger events*, 2008, to appear
- [34] Kachelriess M and Semikoz D V, *Reconciling the ultra-high energy cosmic ray spectrum with Fermi shock acceleration*, 2006 *Phys. Lett.* **B634** 143 [arXiv:astro-ph/0510188]
- [35] Landau L and Lifshitz E, *The classical theory of fields*, 1951, Addison–Wesley
- [36] Longair M S, *High-energy astrophysics. Vol. 1: Particles, photons and their detection*, 1992, Cambridge Univ. Press
- [37] Ostrowski M, *Cosmic ray acceleration at relativistic shocks, shear layers, ...*, 2008, arXiv:0801.1339 [astro-ph]
- [38] Venkatesan A, Miller M C and Olinto A V, *Constraints on the production of ultra-high-energy cosmic rays by isolated neutron stars*, 1997 *Astrophys. J.* **484** 323 [arXiv:astro-ph/9612210]
- [39] Neronov A and Semikoz D, *Particle acceleration and formation of jets in the cores of active galactic nuclei*, 2003 *New Astron. Rev.* **47** 693
- [40] Neronov A, Tinyakov P and Tkachev I, *TeV signatures of compact UHECR accelerators*, 2005 *J. Exp. Theor. Phys.* **100** 656 [arXiv:astro-ph/0402132]
- [41] Neronov A, Semikoz D and Tkachev I, *Ultra-High Energy Cosmic Ray production in the polar cap regions of black hole magnetospheres*, 2007, arXiv:0712.1737 [astro-ph]
- [42] Torres D F and Anchordoqui L A, *Astrophysical origins of ultrahigh energy cosmic rays*, 2004 *Rept. Prog. Phys.* **67** 1663 [arXiv:astro-ph/0402371]
- [43] Gorbunov D and Troitsky S, *A comparative study of correlations between arrival directions of ultra-high-energy cosmic rays and positions of their potential astrophysical sources*, 2005 *Astrop. Phys.* **23** 175 [arXiv:astro-ph/0410741]
- [44] Giovannini M, *The magnetized universe*, 2004 *Int. J. Mod. Phys. D* **13** 391 [arXiv:astro-ph/0312614]
- [45] Vallée J P, *Cosmic magnetic fields - as observed in the Universe, in galactic dynamos, and in the Milky Way*, 2004, *New Astron. Rev.* **48** 763
- [46] Mereghetti S, *The strongest cosmic magnets: Soft Gamma-ray Repeaters and Anomalous X-ray Pulsars*, 2008, arXiv:0804.0250 [astro-ph]

- [47] Bignami G F *et al.*, *The magnetic field of an isolated neutron star from X-ray cyclotron absorption lines*, 2003 *Nature* **423** 725
- [48] Baring M G and Harding A K, *Resonant Compton Upscattering in Anomalous X-ray Pulsars*, 2007 *Astrophys. Space Sci.* **308** 109 [arXiv:astro-ph/0610382]
- [49] Vlemmings W H T, Bignall H E and Diamond P J, *Green Bank Telescope observations of the water masers of NGC 3079: accretion disk magnetic field and maser scintillation*, 2007 *Astrophys. J.* **656** 198 [arXiv:astro-ph/0610912]
- [50] Modjaz M *et al.*, J. M. Moran J M, Kondratko P T and Greenhill L J, *Probing the Magnetic Field at Sub-Parsec Radii in the Accretion Disk of NGC 4258*, 2005 *Astrophys. J.* **626** 104 [arXiv:astro-ph/0502240]
- [51] McCallum, J N, Ellingsen S P, Lovell J E J, *Magnetic field limits and spectral variability in the Circinus galaxy H₂O megamasers*, 2007 *Mon. Not. Roy. Astron. Soc.* **376** 549
- [52] Zavala R T and Taylor G B, *Faraday Rotation Measures in the Parsec-Scale Jets of the Radio Galaxies M87, 3C 111, and 3C 120 2002*, 2002 *Astrophys. J.* **566** L9 [arXiv:astro-ph/0201458]
- [53] Matveenko L I *et al.*, *The Structure of the Nucleus of the Seyfert Galaxy NGC1275*, 1980, *Sov. Astron. Lett.* **6** 42
- [54] Artyukh V S and Chernikov P A, *Physical conditions in the nucleus of the radio galaxy 3C 274*, 2007 *Astron. Rep.* **51** 808
- [55] Tyul'bashev S A, *The Physical Parameters of Several Extragalactic Radio Sources Displaying Rapid Variability*, 2005, *Astron. Rep.* **49** 967
- [56] Chernikov P A *et al.*, *Study of the physical conditions in active galactic nuclei. Physical conditions in the cores of two nearby radio galaxies*, 2006 *Astron. Rep.* **50** 202
- [57] Sligh V I, *Angular Size of Radio Stars*, 1963 *Nature* **199** 682
- [58] Zakharov A F *et al.*, *Magnetic fields in AGNs and microquasars*, 2003 *Mon. Not. Roy. Astron. Soc.* **342** 1325 [arXiv:astro-ph/0212008]
- [59] Gnedin Y M, Natsvlshvili T M and Piotrovich M Y, *Magnetic fields of active galaxy nuclei and cosmological models*, 2005 *Grav. Cosmol.* **11** 333 [arXiv:astro-ph/0509437]
- [60] Znajek R L, *The electric and magnetic conductivity of a Kerr hole*, 1978 *Mon. Not. Roy. Astron. Soc.* **185** 833
- [61] Shakura N I and Syunyaev R A, *Black holes in binary systems. Observational appearance*, 1973 *Astron. Astrophys.* **24** 337
- [62] Novikov I D and Thorne K S, *Astrophysics of black holes*, 1973, in: *Black holes (Les astres occlus)*, Gordon and Breach, p. 343
- [63] Zhang W M, Lu Y and Zhang S N, *The Black Hole Mass and Magnetic Field Correlation in Active Galactic Nuclei*, 2005 *Chin. J. Astron. Astrophys. Suppl.* **5** 347 [arXiv:astro-ph/0501365]
- [64] Paturel G *et al.*, *HYPERLEDA. I. Identification and designation of galaxies*, 2003 *Astron. Astrophys.* **412** 45; <http://leda.univ-lyon1.fr>
- [65] The NASA/IPAC Extragalactic database (available at <http://nedwww.ipac.caltech.edu>).
- [66] Harris D E and Krawczynski H, *X-ray Emission from Extragalactic Jets*, 2006 *Ann. Rev. Astron. Astrophys.* **44** 463 [arXiv:astro-ph/0607228]
- [67] Gallimore J F *et al.*, *A Survey of Kiloparsec-Scale Radio Outflows in Radio-Quiet Active Galactic Nuclei*, 2006 *Astron. J.* **132** 546 [arXiv:astro-ph/0604219]
- [68] Allen, M G *et al.*, *Physical Conditions in the Seyfert Galaxy NGC 2992*, 1999 *Astrophys. J.* **511** 686
- [69] Laine S and Beck R, *Radio Continuum Jet in NGC 7479*, 2008 *Astrophys. J.* **673** 128 [arXiv:0709.4476 [astro-ph]]
- [70] Burns J O, Feigelson E D, Schreier E J, *The inner radio structure of Centaurus A - Clues to the origin of the jet X-ray emission*, 1983 *Astrophys. J.* **273** 128
- [71] Schwartz D A *et al.*, *CHANDRA Observations of X-ray Jet Structure on kpc to Mpc Scales*, 2003 *New Astron. Rev.* **47** 461 [arXiv:astro-ph/0306317]
- [72] Hardcastle M J, Harris D E and Worrall D M, *The origins of X-ray emission from the hotspots of*

- FR II radio sources*, 2004 *Astrophys. J.* **612** 729 [arXiv:astro-ph/0405516]
- [73] Kataoka, J and Stawarz, L, *X-Ray Emission Properties of Large-Scale Jets, Hot Spots, and Lobes in Active Galactic Nuclei*, 2005 *Astrophys. J.* **622** 797
 - [74] Meisenheimer K *et al.*, *The synchrotron spectra of radio hot spot*, 1989 *Astron. Astrophys.* **219** 63
 - [75] Croston J H *et al.*, *An X-ray study of magnetic field strengths and particle content in FR II radio sources*, 2005 *Astrophys. J.* **626** 733 [arXiv:astro-ph/0503203].
 - [76] Vlemmings W H T *et al.*, *The Magnetic Field in the Star-forming Region Cepheus A from Water Maser Polarization Observations*, 2005 arXiv:astro-ph/0510452.
 - [77] Slysh V I and Migenes V, *Strong magnetic field in W75N OH maser flare*, 2006 *Mon. Not. Roy. Astron. Soc.* **369** 1497 [arXiv:astro-ph/0605741]
 - [78] Vlemmings W H T, *A new probe of magnetic fields during high-mass star formation: Zeeman splitting of 6.7 GHz methanol masers*, 2008 *Astron. Astrophys.* **484** 773 [arXiv:0804.1141 [astro-ph]]
 - [79] Sarma A P *et al.*, *VLBA Observations of the Zeeman Effect in H₂O Masers in OH 43.8–0.1*, 2008 *Astrophys. J.* **674** 295
 - [80] Curran R L and Chrysostomou A, *Magnetic fields in massive star forming regions*, 2007 *Mon. Not. Roy. Astron. Soc.* **382** 699 [arXiv:0709.0256 [astro-ph]]
 - [81] Thompson T A *et al.*, *Magnetic Fields in Starburst Galaxies and The Origin of the FIR-Radio Correlation*, 2006 *Astrophys. J.* **645** 186 [arXiv:astro-ph/0601626]
 - [82] Piran T, *Magnetic Fields in Gamma-Ray Bursts: A Short Review*, 2005 *AIP Conf. Proc.* **784** 164 [arXiv:astro-ph/0503060]
 - [83] Waxman E, *Cosmological gamma-ray bursts and the highest energy cosmic rays*, 1995 *Phys. Rev. Lett.* **75** 386 [arXiv:astro-ph/9505082]
 - [84] Vietri M, De Marco D and Guetta D, *On the generation of UHECRs in GRBs: A reappraisal*, 2003 *Astrophys. J.* **592** 378 [arXiv:astro-ph/0302144]
 - [85] Schmidt M, *Luminosities and Space Densities of Gamma-Ray Bursts*, 1999 *Astrophys. J.* **523** L117 [arXiv:astro-ph/9908206]
 - [86] Piran T, *Gamma-Ray Bursts and the Fireball Model*, 1999 *Phys. Rept.* **314** 575 [arXiv:astro-ph/9810256]
 - [87] Govoni F and Feretti L, *Magnetic Field in Clusters of Galaxies*, 2004 *Int. J. Mod. Phys. D* **13** 1549 [arXiv:astro-ph/0410182]
 - [88] Ferrari C *et al.*, *Observations of extended radio emission in clusters*, 2008 *Space Science Reviews*, **134** 93 [arXiv:0801.0985 [astro-ph]]
 - [89] Dolag K *et al.*, *Constrained simulations of the magnetic field in the local universe and the propagation of UHECRs*, 2005 *JCAP* **0501** 009 [arXiv:astro-ph/0410419]
 - [90] Sigl G, Miniati F and Ensslin T A, *Cosmic magnetic fields and their influence on ultra-high energy cosmic ray propagation*, 2004 *Nucl. Phys. Proc. Suppl.* **136** 224 [arXiv:astro-ph/0409098]